scientific reports

Check for updates

OPEN

Study on the antibacterial activity and biocompatibility of nano-silver/carbon nanotube composite coatings on airway stents prepared by micro-transfer printing

Xinhong Huang[1,2,5], Bangzheng Zhu[1,2,5], Keyan Fu[1,2,5], Chengyu Pan[1,2], Tingfang Liu[1,2], Xinhua Yao[3,4]✉ & Jian Ye[1]✉

Common complications following endotracheal intubation or tracheostomy include tracheal stenosis and infection, which often exacerbate one another, complicating treatment. In this context, airway stents with stable antimicrobial properties and excellent biocompatibility emerge as an ideal therapeutic option. Silver nanoparticles (AgNPs) are renowned for their remarkable antibacterial and anti-inflammatory activities, making their incorporation into airway stent coatings a promising strategy for addressing stent-associated infections and granulation tissue proliferation. In preliminary research, a silicone airway stent coated with a Silver nanoparticles/Carbon nanotubes (AgNPs/CNTs) layer was successfully fabricated, and the present study was conducted to further evaluate its antimicrobial properties and tissue compatibility through systematic in vitro and in vivo experiments. In vitro experiments assessed its antimicrobial properties using the paper disc agar diffusion method and bacterial co-cultivation assay, with the bacteriostatic effect quantified through bacterial counting. For in vivo experiments, a New Zealand rabbit model was employed, wherein AgNPs/CNTs-coated airway stents were implanted alongside standard silicone stents. Tracheal lavage was performed at two and four weeks post-surgery, followed by colony counting. Additionally, histological evaluations were conducted to assess inflammation, granulation tissue proliferation, and collagen deposition, while confocal microscopy was used to observe and measure biofilm formation on the surface of the airway stents. The in vitro antimicrobial zone tests demonstrated that the AgNPs/CNTs coating effectively inhibited the growth of *Staphylococcus aureus* and *Pseudomonas aeruginosa*, with inhibition zones measuring 17.13 ± 1.21 mm and 13.55 ± 0.81 mm, respectively. In the bacterial co-cultivation assay, the AgNPs/CNTs group exhibited significantly fewer colony counts compared to the standard silicone group ($P < 0.05$). In vivo antimicrobial experiments revealed that the colony count in the AgNPs/CNTs-coated group was significantly lower than that of the standard silicone group at both the 2-week and 4-week time points ($P < 0.05$). Histological analysis under microscopy indicated that the AgNPs/CNTs group had significantly reduced granulation tissue thickness, inflammatory cell infiltration, and collagen deposition compared to the standard silicone group ($P < 0.05$). Furthermore, confocal microscopy measurements of biofilm formation revealed that the biofilm thickness on the surface of the AgNPs/CNTs-coated stents was 25.75 ± 5.93 µm, significantly lower than the 45.27 ± 12.84 µm observed on the standard silicone stents ($P < 0.05$). The AgNPs/CNTs-coated airway stent exhibited exceptional antimicrobial properties both in vitro and in vivo, effectively inhibiting bacterial growth, reducing bacterial colonization and biofilm formation within the airway, and significantly alleviating granulation tissue proliferation and collagen deposition. This, in turn, improved the airway microenvironment. This study provides a theoretical foundation for the clinical application of AgNPs/CNTs-coated airway stents.

Keywords Airway stent, Silver nanoparticles, Carbon nanotubes, Antibacterial activity, Biocompatibility

Abbreviations

AgNPs Silver nanoparticles

CNTs	Carbon nanotubes
MWCNTs	Carboxylated multi-walled carbon nanotubes
FDM	Fused deposition modeling
PDMS	Polydimethylsiloxane
LSR	Liquid silicone rubber
HE	Hematoxylin-eosin
MTS	Masson's trichrome

[1]Department of Respiratory Medicine, Zhejiang Hospital, Hangzhou, Zhejiang, China. [2]Zhejiang Chinese Medical University, Hangzhou, Zhejiang, China. [3]The State Key Laboratory of Fluid Power and Mechatronic Systems, College of Mechanical Engineering, Zhejiang University, Hangzhou, China. [4]Key Laboratory of 3D Printing Process and Equipment of Zhejiang Province, College of Mechanical Engineering, Zhejiang University, Hangzhou, China. [5]Xinhong Huang, Bangzheng Zhu, and Keyan Fu contributed equally to this work. ✉email: yaoxinhuame@zju.edu.cn; yejianchi@126.com

Airway stenosis is typically caused by local or systemic inflammation, tuberculosis, tumors, and other factors, which can obstruct airflow, leading to respiratory distress and, in severe cases, even endanger life. Treatment options for airway stenosis include pharmacotherapy, surgical resection, and interventional procedures such as stent placement, balloon dilation, thermal ablation, and cryotherapy[1]. Among these, stent implantation can accurately expand the narrowed airway and rapidly relieve the resulting respiratory distress, offering greater safety and maneuverability compared to other treatment options. With the continuous advancement of interventional techniques and airway stents, stent implantation has become an increasingly common therapeutic choice. Currently, silicone and metal stents are the most widely used types in the treatment of airway stenosis. However, studies have shown that the incidence of complications after airway stent implantation can be as high as 15%, with long-term users being particularly susceptible. Common complications include granulation tissue formation, infection, and restenosis, all of which are significant factors affecting patient prognosis[2,3].

Stent implantation inevitably exerts pressure and causes damage to surrounding tissues, stimulating granulation tissue formation and leading to local circulatory disturbances, particularly in regions where mechanical stress at both ends of the stent is higher. This results in a decline in the airway's ability to contract and expand during the respiratory cycle[4]. Furthermore, when the stent is embedded in the tracheal mucosa, it may disrupt the cleaning function of the bronchial epithelium cilia in the stented segment, leading to the accumulation of secretions and bacterial aggregation, thereby increasing the risk of respiratory infections. Studies indicate that within 3–4 weeks after stent implantation, the bacterial colonization rate in the airway can reach 78%, with common pathogens including *Staphylococcus aureus, Pseudomonas aeruginosa, and Escherichia coli*[5]. Additionally, prolonged bacterial colonization on the stent surface can lead to biofilm formation, further elevating the risk of drug-resistant bacteria and refractory respiratory infections[6]. Notably, a synergistic relationship exists between granulation tissue proliferation and airway infection. Infections caused by the stent can promote pathological healing of surrounding wounds and granulation tissue growth, ultimately leading to airway restenosis, further hindering secretion drainage and exacerbating bacterial accumulation, thereby increasing the risk of infection. Therefore, developing airway stents with inherent anti-infection capabilities presents an effective solution to address these issues.

The antimicrobial, anti-inflammatory, antioxidant, and anticancer properties of various nanoparticles and microparticles have been extensively studied. Silver nanoparticles (AgNPs) as a substance with both antimicrobial and anti-inflammatory activities, play a crucial role in infection treatment. As a nonspecific bactericide, silver nanoparticles, at appropriate doses, are non-toxic to mammalian cells and can effectively inhibit a wide range of bacteria and fungi, including antibiotic-resistant strains[7]. However, free AgNPs tend to aggregate in aqueous solutions, significantly reducing their bactericidal efficacy. To address this issue, CNTs materials, which have emerged in recent years, are considered an excellent carrier for AgNPs due to their unique nanostructure, large surface area, and other superior physicochemical properties. Relevant studies have shown that Silver nanoparticles/Carbon nanotubes (AgNPs/CNTs) exhibit strong antimicrobial activity[8,9]. Contemporary medical research has confirmed the favorable therapeutic efficacy of silicone stents in the management of traumatic tracheal stenosis[10]. The integration of 3D printing technology enables the design of patient-specific stents tailored to individual anatomical features. Such customized 3D-printed stents not only enhance the precision of airway conformity but also improve compliance, thereby effectively reducing the risk of potential complications such as stent migration and granulation tissue hyperplasia[11].

Silicone, also known as silicone rubber, is a class of biocompatible, non-degradable, inert synthetic polymer elastomers. Due to their excellent biocompatibility, biological durability, and mechanical properties such as high strength and elasticity, silicones are widely used in the production of various medical products. However, the relatively low surface energy of silicone materials results in poor adhesion of antimicrobial agents to their surfaces, significantly limiting the application of antimicrobial coatings. As shown in Fig. 1, this study employs 3D printing technology, using silicone as ink to create airway stent models. AgNPs-modified CNTs are synthesized as antimicrobial agents through in situ reduction and, combined with the micro-transfer printing process, the nano-antimicrobial coating is fixed onto the stent surface. The aim is to develop airway stents with both antimicrobial properties and good tissue compatibility. Preliminary studies have shown, through scanning electron microscopy, that AgNPs are evenly distributed on the surface of CNTs. Adhesion tests with adhesive tape and UV–visible spectroscopy have demonstrated the strong attachment of AgNPs/CNTs on silicon substrates. The objective of this research is to further evaluate the antibacterial and anti-granulation tissue proliferation properties of this novel airway stent, to provide valuable insights for clinical practice and future airway stent research.

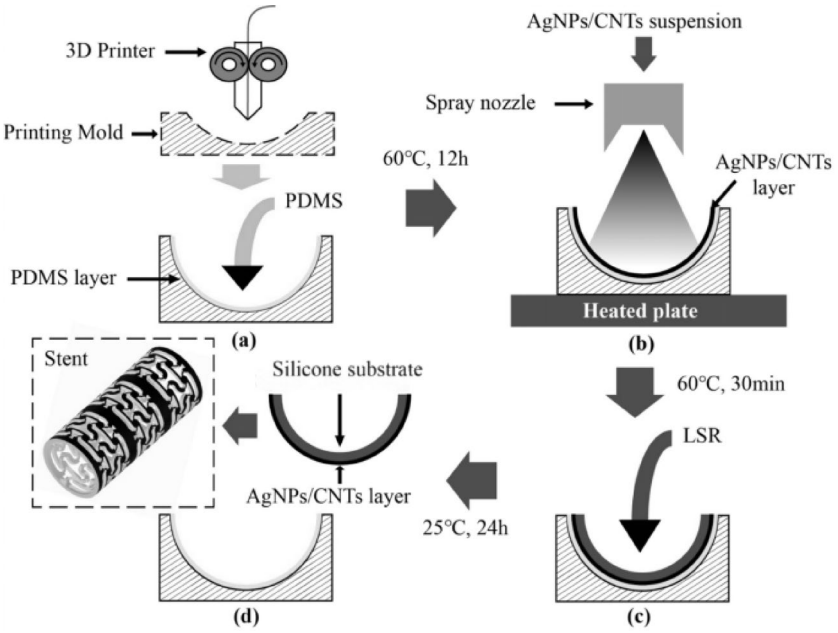

Fig. 1. Schematic Diagram of the 3D Printing AgNPs/CNT Coating Spraying-Transfer Proces. (**a**) Fabricate the mold using a 3D printer, then apply a thin layer of polydimethylsiloxane (PDMS). (**b**) Deposit the AgNPs/CNTs layer onto the PDMS surface via spray deposition. (**c**) Pour liquid silicone rubber into the mold. (**d**) Peel the silicon substrate coated with the AgNPs/CNTs layer from the PDMS. The image within the rectangle depicts the model of the AgNPs/CNTs-coated silicone resin tracheal stent.

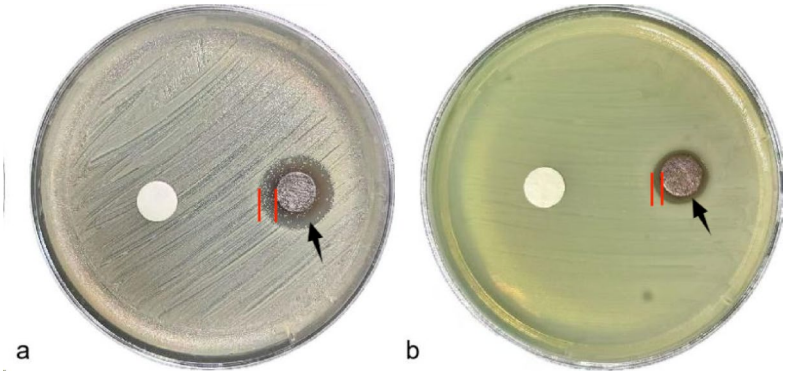

Fig. 2. In Vitro Agar Plate Diffusion Experiment Diagram (**a**) On the right, a clear halo of inhibition is visible around the disc soaked in AgNPs/CNTs solution on the *Staphylococcus aureus*-inoculated plate, indicating effective antibacterial activity. In contrast, the control disc on the left, immersed in physiological saline, shows no such halo, with normal bacterial growth surrounding it; (**b**) Similarly, on the right side of the *Pseudomonas aeruginosa*-inoculated plate, the AgNPs/CNTs disc exhibits a distinct transparent zone of inhibition, while the control disc on the left is surrounded solely by green bacterial colonies, with no evidence of inhibition.

Results

Antibacterial study of AgNPs/CNTs coated airway stents

In vitro agar diffusion method for antibacterial effect evaluation

The results of the agar-plate diffusion experiment showed that the AgNPs/CNTs group exhibited significant growth inhibition against both *Staphylococcus aureus* and *Pseudomonas aeruginosa* (Fig. 2). The average diameters of the inhibition zones for *Staphylococcus aureus* and *Pseudomonas aeruginosa* were 17.13 ± 1.21 mm and 13.55 ± 0.81 mm, respectively, while the silicone-only group showed no distinct inhibition zones, indirectly indicating that the silver nanoparticles possess excellent antimicrobial activity.

In vitro co-culture and plate colony counting methods for antibacterial testing

Through co-culture and bacterial plate colony formation experiments, the antibacterial effect was quantitatively analyzed in vitro. After 24 h of co-culturing AgNPs/CNTs with *Staphylococcus aureus* suspension, the colony

count formed on nutrient agar plates was $(5.89 \pm 1.60) \times 10^{10}$ CFU/mL, compared to the silicone-only group $(17.33 \pm 2.92) \times 10^{10}$ CFU/mL ($P < 0.05$). After 24 h of co-culturing with *Pseudomonas aeruginosa*, the colony count was $(4.44 \pm 1.67) \times 10^{10}$ CFU/mL, compared to the silicone-only group $(9.89 \pm 1.90) \times 10^{10}$ CFU/mL ($P < 0.05$), as shown in Fig. 3. The antibacterial rates of AgNPs/CNTs against *Staphylococcus aureus* and *Pseudomonas aeruginosa* were 66.01% ± 19.21% and 55.11% ± 25.58%, respectively. These results indicate that AgNPs/CNTs are an effective antimicrobial nanocomposite material.

Comparison of antibacterial effects in rabbit airway stent models

As shown in Fig. 4, both in the second and fourth weeks, the colony distribution on the plates from the silicone-only group was denser than that of the AgNPs/CNTs group. Further colony counting results revealed that in the second week, the bacterial colony count on nutrient agar plates for the AgNPs/CNTs group was $(0.47 \pm 0.19) \times 10^5$ CFU/mL, significantly lower than the $(1.27 \pm 0.33) \times 10^5$ CFU/mL of the silicone-only group ($P < 0.05$). In the fourth week, the bacterial colony count for the AgNPs/CNTs group was $(3.19 \pm 0.73) \times 10^5$ CFU/mL, also significantly lower than the $(5.61 \pm 0.98) \times 10^5$ CFU/mL of the silicone-only group ($P < 0.05$). Mass spectrometry analysis indicated the bacterial species distribution in the airway, which were as follows: *Escherichia coli*(28.57%), *Pseudomonas aeruginosa*(23.81%), *Staphylococcus aureus*(14.29%), *Pasteurella spp.*(14.29%), *Proteus spp.* (9.52%), and other genera (9.52%), as shown in Fig. 5.

Biofilm thickness measurement

As shown in Fig. 6, when the airway stents were removed in the fourth week, the inner lumen of the silicone-only stent was found to be obstructed by a large amount of purulent white secretion, while only a small amount of airway secretion was adhered to the surface of the AgNPs/CNTs-coated stent. According to Cotton's stenosis grading system[12], the stenosis grade of the silicone-only group was predominantly grade II and above, whereas the stenosis degree of the AgNPs/CNTs-coated group was grade I and below. Further Fluorescein-labeled Concanavalin A (FITC-ConA) staining and dark treatment of biofilms, followed by confocal microscopy observation, were used to measure the biofilm thickness on the stents. The results showed that the biofilm thickness on the AgNPs/CNTs group was 25.75 ± 5.93 μm, significantly lower than the 45.27 ± 12.84 μm observed in the silicone-only group ($P < 0.05$), as shown in Fig. 7.

Biocompatibility study of AgNPs/CNTs coated airway stents

Evaluation of AgNPs/CNTs coating on granulation tissue proliferation

At the designated time points (second and fourth weeks), tracheal specimens were collected from the proximal or distal ends of the airway stents for H&E staining and Masson staining. As shown in Fig. 8, in the second week, epithelial cell proliferation was significantly observed in the trachea of the silicone-only group. By the fourth week, distinct granulation tissue was visible in the trachea of the silicone-only group. In contrast, the progression

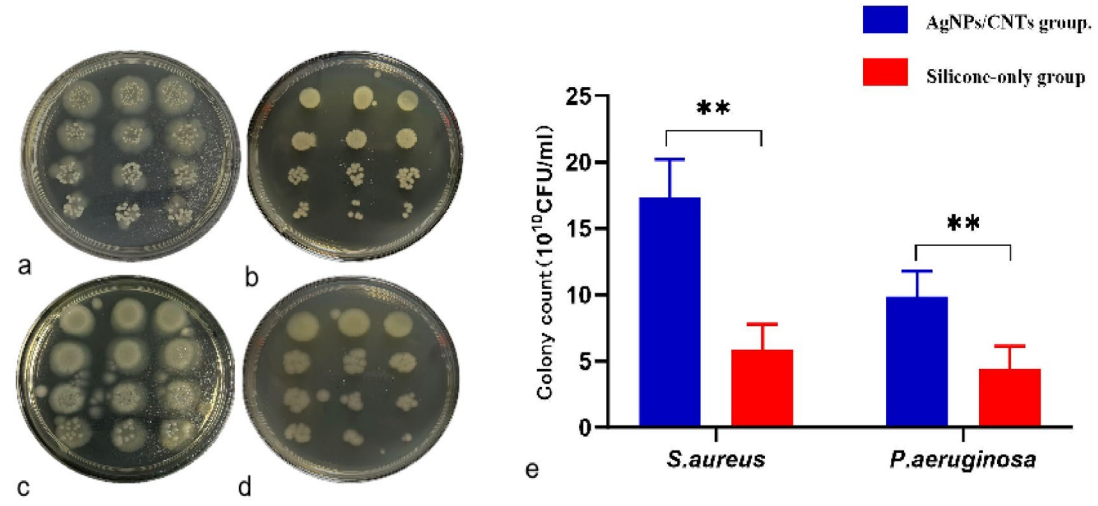

Fig. 3. The in vitro colony count after co-cultivation followed by tenfold serial dilution culture. (**a**) After co-cultivation of *Staphylococcus aureus* with ordinary silicone materials, followed by tenfold serial dilution plate culture, the colony distribution is dense, and the number is relatively high; (**b**) After co-cultivation of *Staphylococcus aureus* with AgNPs/CNTs materials, followed by tenfold serial dilution plate culture, the colony distribution is sparse, and the bacterial count is relatively low; (**c**) After co-cultivation of *Pseudomonas aeruginosa* with ordinary silicone materials, followed by tenfold serial dilution plate culture, the colony distribution is dense, and the bacterial count is relatively high; (**d**) After co-cultivation of *Pseudomonas aeruginosa* with AgNPs/CNTs materials, followed by tenfold serial dilution plate culture, the colony distribution is sparse, and the bacterial count is relatively low; (**e**) Statistical comparison of colony numbers between the ordinary silicone group and the AgNPs/CNTs group. *Note* Dilution gradient to 10^{-8}, $^{*}P < 0.05$ and $^{**}P < 0.005$.

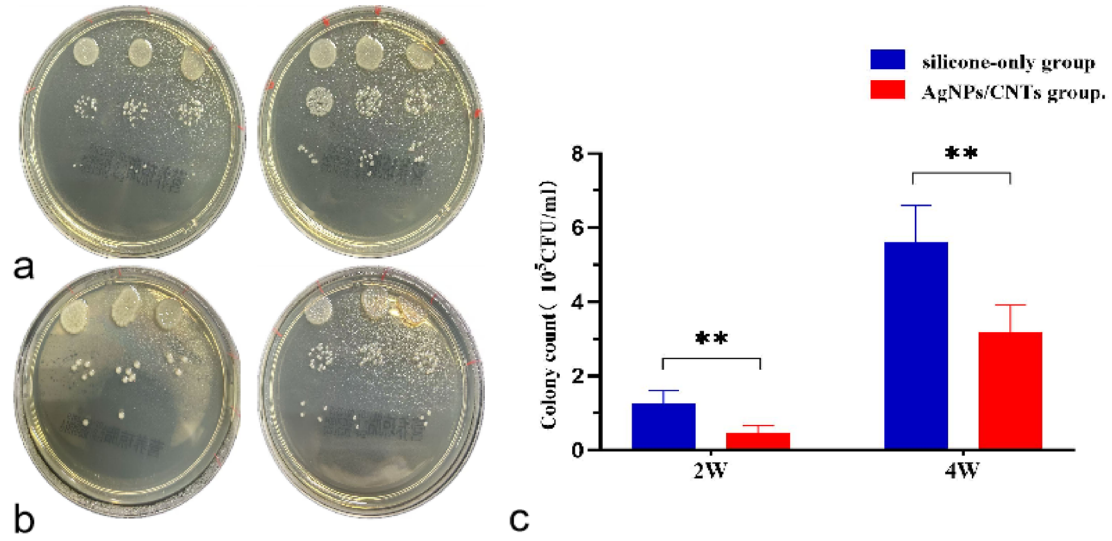

Fig. 4. Colony culture and statistical comparison after tracheal stent implantation. (**a**) Plate colony formation images after ordinary silicone stent implantation in the trachea for 2 weeks and 4 weeks; (**b**) Plate colony formation images after AgNPs/CNTs-coated stent implantation in the trachea for 2 weeks and 4 weeks, showing that the number of colonies gradually increases with the duration of stent implantation;(**c**) Statistical comparison of colony numbers after 2 weeks and 4 weeks of stent implantation in the two groups. *Note* Dilution gradient to 10^{-3}, $^{*}P<0.05$ and $^{**}P<0.005$.

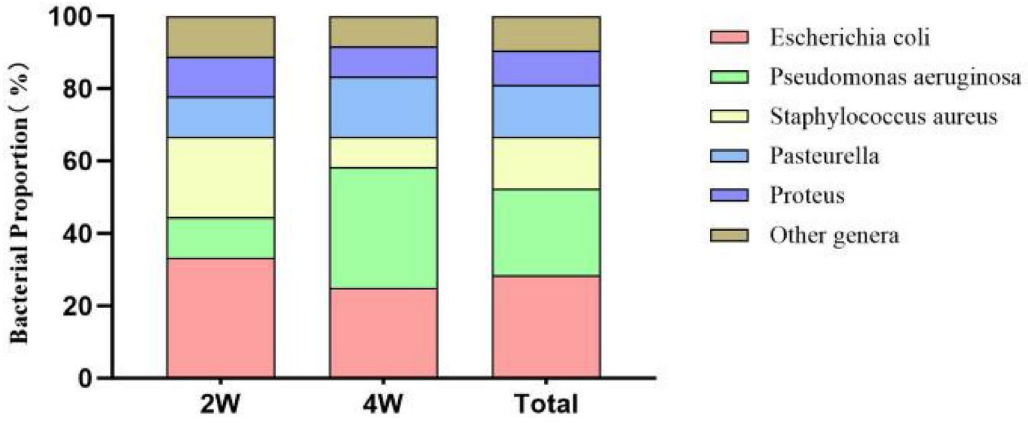

Fig. 5. Bacterial species composition ratio.

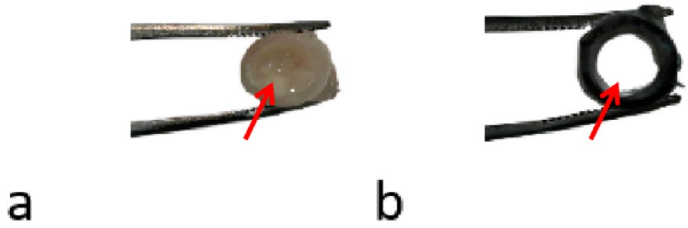

Fig. 6. Lumen image after 4 weeks of scaffold implantation. (**a**) Ordinary silicone scaffold, with the lumen filled with mucus; (**b**) AgNPs/CNTs-coated scaffold, with a small amount of mucus adhering to the tube wall.

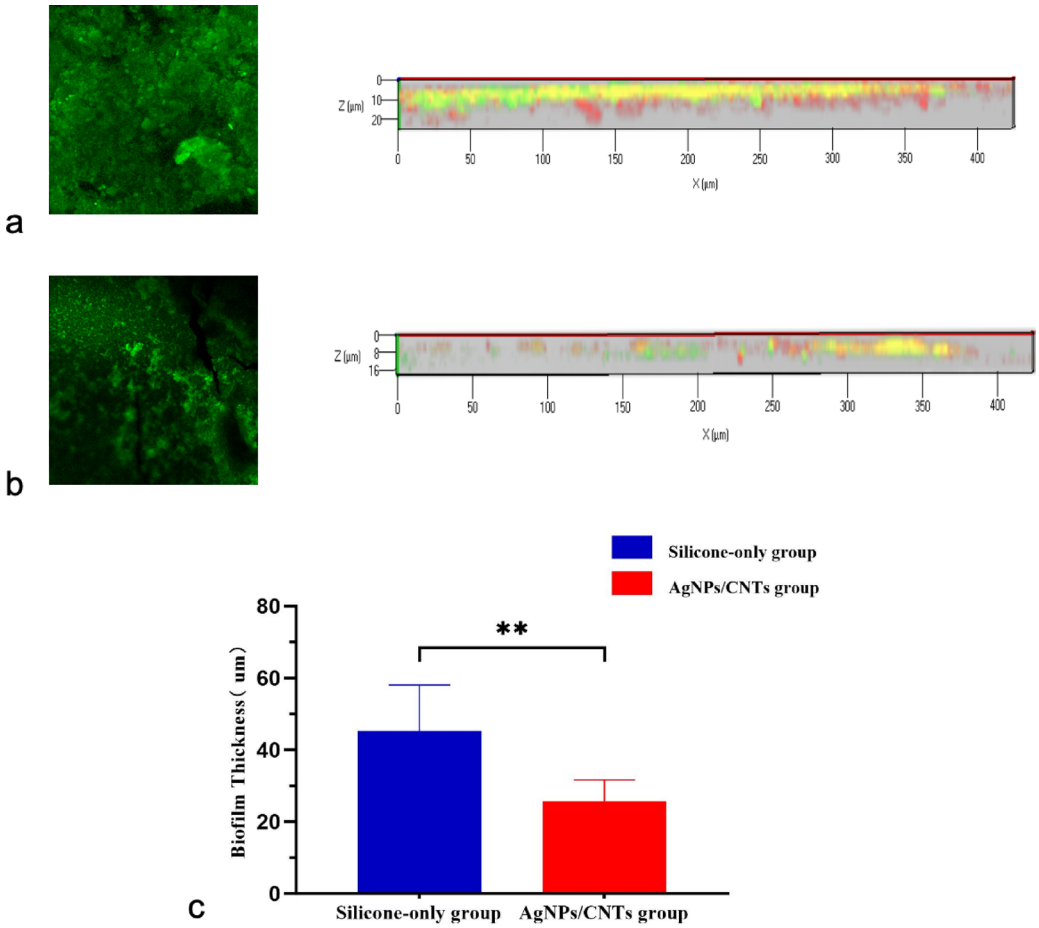

Fig. 7. Comparison of biofilms after implantation of ordinary silicone stents and AgNPs/CNTs-coated stents for 4 weeks. (**a**) Biofilm morphology and three-dimensional configuration images of the ordinary silicone stent under a confocal microscope. The biofilm on the surface of the ordinary silicone stent is deeply stained and densely distributed, and the three-dimensional reconstruction shows a relatively large thickness; (**b**) Biofilm morphology and three-dimensional configuration images of the AgNPs/CNTs-coated stent under a confocal microscope. The biofilm on the surface of the AgNPs/CNTs-coated stent is lightly stained and sparsely distributed, and the three-dimensional reconstruction shows a relatively small thickness; (**c**) Statistical comparison of biofilm thickness between the two groups ($P < 0.005$).

of epithelial cells and granulation tissue in the AgNPs/CNTs-coated group was slower at the same time points. The extent of inflammatory cell infiltration in the two groups was 4.38 ± 0.12 and 3.67 ± 0.16, respectively ($P < 0.05$), as shown in Fig. 8d. The statistical analysis in Fig. 8e showed that, compared to the silicone-only group (562.97 ± 41.34 μm), the granulation tissue thickness in the AgNPs/CNTs-coated group was significantly reduced to (404.98 ± 43.30 μm). Collagen, a major component of the extracellular matrix, can lead to airway restenosis if excessively deposited. The collagen deposition in the silicone-only group was $28.45\% \pm 1.02\%$, whereas in the AgNPs/CNTs-coated group, it was significantly lower at $18.90\% \pm 1.06\%$, indicating that the AgNPs/CNTs coating can significantly inhibit collagen deposition, as shown in Fig. 8f.

Correlation analysis between bacterial load and tracheal granulation tissue proliferation in rabbit airway models
To investigate whether infection promotes granulation tissue formation, this study conducted a correlation analysis between bacterial content and tracheal granulation tissue proliferation following tracheal stent implantation in rabbits. The results revealed a positive correlation between bacterial content in the airway and the proliferation of granulation tissue (as shown in Fig. 9). Specifically, higher microbial content on the surface of the stent was associated with a more pronounced proliferation of granulation tissue within the airway.

Discussion and conclusion

Airway stent implantation, as a crucial component of respiratory interventional techniques, is widely used in the treatment of diseases such as tracheal and bronchial stenosis, as well as fistulas. Its advantages include minimal trauma, short treatment time, and rapid recovery, effectively supporting stenotic airways and promptly restoring patency[13]. However, complications following stent implantation have long been a challenge in clinical practice, representing major issues that need urgent resolution. These complications include granulation tissue formation

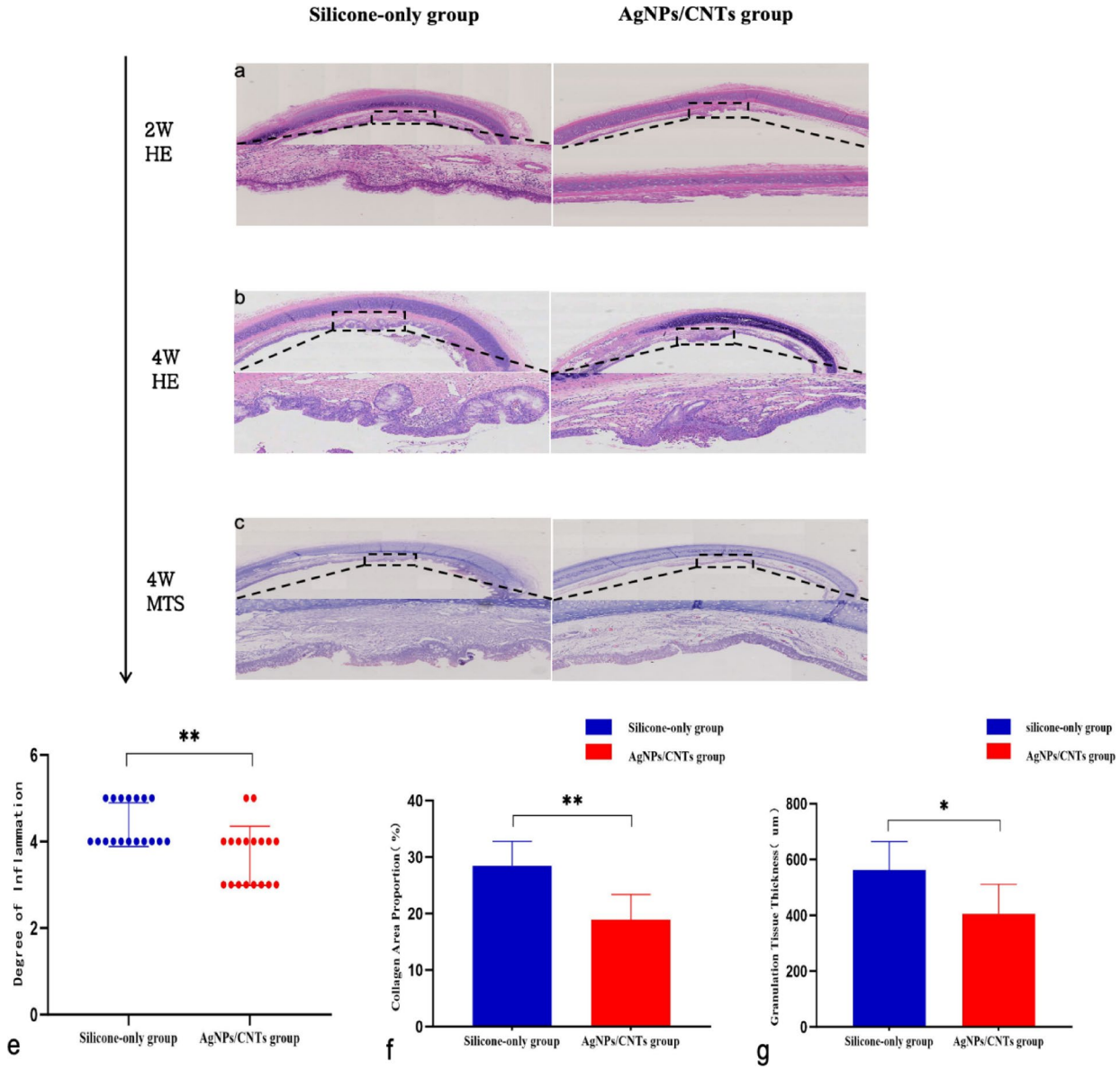

Fig. 8. Histological staining images and statistical comparison after stent implantation in the trachea. (**a**) Histological HE staining of tracheal tissue 2 weeks after airway stent placement; (**b**) Histological HE staining of tracheal tissue 4 weeks after airway stent placement; (**c**) Histological MTS staining of tracheal tissue 4 weeks after airway stent placement; (**d**) Statistical comparison of the degree of inflammatory infiltration between the two groups; (**e**) Statistical comparison of granulation tissue thickness between the two groups; (**f**) Statistical comparison of collagen area percentage between the two groups. *Note* $^{*}P<0.05$ and $^{**}P<0.005$.

leading to airway restenosis, respiratory infections, and stent encasement or impaction[2,3]. The respiratory system, being directly connected to the external environment, is the most common site for microbial colonization. The normal human respiratory tract harbors various symbiotic microbial communities that interact with each other to maintain a stable state, typically without pathogenicity. However, after stent implantation, the original dynamic balance is disrupted, leading to dysbiosis. Opportunistic pathogens such as *Streptococcus pneumoniae*, *Haemophilus influenzae*, and *Moraxella catarrhalis* may cause infections. A systematic review of 501 airway stent patients found that the incidence of stent-related respiratory infections was as high as 19%, with the most common infection type being pneumonia, and the most frequent pathogens being *Staphylococcus aureus*, *Pseudomonas aeruginosa*, and *Escherichia coli*[14]. Furthermore, the formation of bacterial biofilms on the surface of airway stents is considered one of the key factors in uncontrolled infection. Biofilms provide a protective barrier for bacteria, hindering phagocytic function, resisting host immune responses, and weakening the effects of fluid shear forces and antimicrobial agents[6,15]. The long-term adverse reaction between the tracheal stent and microorganisms accelerates the formation of bacterial biofilms[16]. A prospective study showed that 3 to 4 weeks after airway stent implantation, the biofilm colonization rate in the stent reached 78%, with pathogenic bacteria detected in 55% of the biofilm-colonized patients[17]. Another molecular investigation on airway stent biofilms

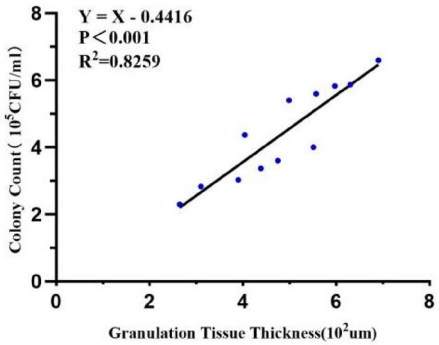

Fig. 9. Linear correlation between bacterial load and granulation tissue proliferation.

found that pathogens within bacterial biofilms are more resistant to host immunity and antimicrobial drugs than other bacterial forms. Lipid-containing bacterial biofilms impede the penetration of water-soluble antibiotics, making common antibiotic treatments less effective against biofilm-induced infections[18,19].

The process of airway tissue damage repair and the granulation tissue hyperplasia triggered by inflammatory stimuli are the primary causes of airway restenosis. On one hand, airway stents, as foreign bodies that remain in the human body for extended periods, inevitably provoke immune rejection reactions and chronic inflammation. In this inflammatory environment, inflammatory cells and cytokines interact, promoting the proliferation of fibroblasts and capillaries. In the early stages of inflammation, fibroblasts support the survival of other inflammatory cells by providing extracellular matrix and connective tissue, while producing collagen, ultimately leading to scar tissue formation and subsequent airway restenosis. On the other hand, the inflammatory factors and anti-inflammatory factors induced by tissue damage are activated or suppressed along a temporal axis, while neutrophils, macrophages, and T cells are recruited to the inflammatory site to clear necrotic tissue and facilitate repair. However, when these regulatory processes are disrupted, the inflammatory response leads to overexpression of fibroblast growth factors, collagen, and α-smooth muscle actin, stimulating fibroblast proliferation and differentiation. This results in excessive extracellular matrix accumulation and the onset of granulation tissue hyperplasia within the airway[18]. Moreover, bacterial infections and proliferation in the trachea play a significant role in granulation tissue formation. After airway stent implantation, the tracheal wall in contact with the stent becomes congested and swollen, with plasma exudates forming a membranous substance that adheres to the airway wall, promoting mucus retention and infection. A study by Sasak demonstrated a positive correlation between bacterial colonization and granulation tissue formation after stent implantation[16]. Simoni analyzed the microbial infections following stent placement and found that controlling local bacterial infections helps inhibit the formation of granulation tissue in the airway[5]. Therefore, unlike the sterile environment within blood vessels, airway stents with dual properties of anti-infection and anti-proliferation may be more effective in suppressing airway restenosis.

Since ancient Greece, the antimicrobial properties of silver (Ag) have been well known. Among the commonly used inorganic antimicrobial agents, silver is one of the most effective and widely applied, with significant antimicrobial activity. As a broad-spectrum antimicrobial agent, silver can target over 650 types of bacteria and fungi, far surpassing organic antimicrobial agents like antibiotics[20]. In recent years, with the advancement of nanotechnology, scientists have discovered that various nanoparticles and microparticles exhibit antimicrobial, anti-inflammatory, and antioxidant properties. The antimicrobial performance of nanoparticles is influenced by their size; smaller nanoparticles can more efficiently bind to bacterial surfaces and penetrate cell membranes, thereby killing the bacteria[21]. AgNPs possess a large specific surface area, making them more susceptible to oxidation and releasing silver ions, thus becoming a new option for silver-based antimicrobial coatings. Studies have shown that AgNPs exhibit significant antimicrobial or bactericidal effects against both Gram-positive and Gram-negative bacteria. Their antimicrobial mechanism primarily involves damaging the cell wall and membrane, DNA damage, inducing oxidative stress, and inhibiting essential functional proteins[22,23]. In terms of antibiofilm activity, AgNPs inhibit bacterial adhesion, suppress quorum sensing, and reduce the expression of biofilm-related genes, thus exerting their antibiofilm effect[24–26]. Ansari observed through scanning electron microscopy that AgNPs can destroy bacterial structures, causing deep pits and holes in the biofilm[27]. Several studies have indicated that AgNPs coated on biliary stents effectively inhibit bacterial adhesion and subsequent biofilm formation, reducing the risk of stent-associated infections and restenosis[28,29]. However, free AgNPs tend to aggregate in aqueous solutions, which diminishes their antimicrobial effectiveness. To address this issue, CNTs, due to their unique nanostructure, large surface area, and excellent physicochemical properties, have emerged as an ideal support material[8,9]. Conventional airway stents are typically tubular structures with circular cross-sections, which fail to capture the individualized anatomical characteristics of the human airway. Incomplete contact between the stent and the tracheal wall may lead to stent displacement and excessive granulation tissue formation, while non-contact areas provide a favorable niche for bacterial colonization. The use of 3D printing to fabricate personalized stents tailored to the intricate morphology of the airway significantly mitigates these complications by enhancing anatomical conformity and reducing regions susceptible to microbial growth[30]. Therefore, in this study, 3D printing technology combined with spray coating and transfer printing techniques

was used to fabricate airway stents coated with AgNPs/CNTs, aiming to reduce the incidence of stent-associated airway infections and alleviate the extent of granulation tissue hyperplasia.

This study qualitatively and quantitatively assessed the antimicrobial and bactericidal properties of AgNPs/CNTs coatings through in vitro antimicrobial circle and plate colony counting experiments. On plates inoculated with *Staphylococcus aureus* and *Pseudomonas aeruginosa*, the AgNPs/CNTs group formed clear circular halos around the colonies, with widths of 17.13 ± 1.21 mm and 13.55 ± 0.81 mm, respectively. In contrast, the regular silicone group showed no visible clear halos, with only yellow-white or green colonies surrounding the inoculation sites. This preliminary observation suggested that AgNPs/CNTs possess antimicrobial ability. Further, AgNPs/CNTs and regular silicone were separately incubated in Luria–Bertani (LB) suspensions with a bacterial concentration of 10^6 CFU/mL, co-cultured with the two bacterial strains. After sampling, serial dilutions were plated on nutrient agar to quantify the remaining viable bacteria. Visual inspection showed that the bacterial colonies formed by the AgNPs/CNTs group were more sparse than those formed by the control group. Image analysis software revealed that after co-culturing with *S. aureus* for 24 h, the AgNPs/CNTs group formed $(5.89 \pm 1.60) \times 10^{10}$ CFU/mL on nutrient agar, while the control group formed $(17.33 \pm 2.92) \times 10^{10}$ CFU/mL ($P < 0.05$). For *P. aeruginosa*, after 24 h of co-culturing, the AgNPs/CNTs group formed $(4.44 \pm 1.67) \times 10^{10}$ CFU/mL, significantly fewer than the control group's $(9.89 \pm 1.90) \times 10^{10}$ CFU/mL ($P < 0.05$). The inhibition rates of AgNPs/CNTs against *S. aureus* and *P. aeruginosa* were $66.01\% \pm 19.21\%$ and $55.11\% \pm 25.58\%$, respectively. These results indicate a significant difference in antimicrobial properties between the AgNPs/CNTs and the regular silicone group. To further simulate the changes in the airway microenvironment following stent implantation, the study established a rabbit tracheal stent implantation model. Bronchoalveolar lavage fluid was collected at predetermined time points for plate colony counting to evaluate antimicrobial performance. The results showed that at both 2 weeks and 4 weeks, the colony density on the plates from the regular silicone group was significantly higher than that of the AgNPs/CNTs group. At 2 weeks, the AgNPs/CNTs group formed $(0.47 \pm 0.19) \times 10^5$ CFU/mL on nutrient agar, significantly lower than the regular silicone group's $(1.27 \pm 0.33) \times 10^5$ CFU/mL ($P < 0.05$). At 4 weeks, the AgNPs/CNTs group formed $(3.19 \pm 0.73) \times 10^5$ CFU/mL, also significantly lower than the regular silicone group's $(5.61 \pm 0.98) \times 10^5$ CFU/mL ($P < 0.05$). Additionally, at the same time points, the tracheal stents were analyzed. The regular silicone group had a substantial amount of purulent white secretion blocking the lumen, and the stent narrowing was predominantly grade II or higher, while the AgNPs/CNTs-coated stent showed only minimal airway secretion and maintained a narrowing grade of I or below. FITC-ConA staining and confocal microscopy were used to measure biofilm thickness on the airway stent surfaces. The biofilm thickness on the AgNPs/CNTs group was 25.75 ± 5.93 μm, significantly thinner than the regular silicone group's 45.27 ± 12.84 μm ($P < 0.05$). In conclusion, both in vitro and in vivo antimicrobial studies demonstrate that AgNPs/CNTs-coated stents possess excellent antimicrobial activity, providing a strong reference for their potential clinical application.

This study collected tracheal specimens from the proximal and distal ends of airway stents at predetermined time points for HE and Masson staining, aiming to evaluate tissue proliferation in terms of granulation tissue thickness, inflammatory cell infiltration, and collagen deposition. At the 2-week time point, significant epithelial hyperplasia was observed in the tracheas of the regular silicone stent group. By the 4th week, marked granulation tissue formation was evident. In contrast, the epithelial cell proliferation and granulation tissue progression in the AgNPs/CNTs-coated group were slower. Upon measuring tissue sections stained with HE, the granulation tissue thickness in the AgNPs/CNTs group was 404.98 ± 43.30 μm, significantly lower than the 562.97 ± 41.34 μm observed in the regular silicone group ($P < 0.05$). Furthermore, inflammatory cell infiltration was evaluated by counting the cells in HE-stained sections, with the AgNPs/CNTs group showing an infiltration score of 3.72 ± 0.16, significantly lower than the 4.38 ± 0.12 observed in the regular silicone group ($P < 0.05$). Masson staining images showed that the collagen deposition in the regular silicone group was $28.45\% \pm 1.02\%$, while in the AgNPs/CNTs-coated group, it was $18.90\% \pm 1.06\%$, indicating that AgNPs/CNTs coatings significantly reduced collagen deposition ($P < 0.05$). These results suggest that AgNPs/CNTs coatings effectively reduce tracheal inflammation after stent implantation, significantly inhibit granulation tissue formation, and suppress collagen deposition, demonstrating excellent anti-inflammatory and anti-proliferative properties. Additionally, to explore whether infection contributes to granulation tissue formation, the correlation between bacterial content and tracheal granulation tissue growth was analyzed. As shown in Fig. 9, there was a positive correlation between microbial content in the airway and granulation tissue thickness in the tracheal mucosa. By inhibiting microbial proliferation in the airway and improving the tracheal microenvironment, the occurrence of granulation tissue formation can be reduced, which may positively affect stent patency. However, some researchers have raised concerns about the toxicity and safety of AgNPs. In fact, the toxicity of AgNPs depends on factors such as material, shape, and distribution. Most AgNPs that accumulate in organs can be cleared within 8 weeks[31,32]. Furthermore, AgNPs at safe doses have been widely used in food packaging, wound dressings, and medical devices, showing high safety levels. Liu reported that the silver nanoparticle/carbon nanotube antibacterial coatings fabricated via a printing–spraying–transfer process exhibited good biocompatibility with human bronchial epithelial cells in the CCK-8 assay. The cell viability on the mold-transferred coatings was comparable to that of the control group, whereas the sprayed coatings significantly inhibited cell proliferation, likely due to surface roughness and instability[33].

In conclusion, airway stent implantation plays a crucial role in the treatment of tracheal and bronchial stenosis and related diseases. However, its complications, particularly bacterial infections and airway restenosis, remain major clinical challenges. As a broad-spectrum antimicrobial material, AgNPs have demonstrated significant effects in inhibiting bacterial biofilm formation, reducing infections, and alleviating granulation tissue proliferation. This study, by combining AgNPs/CNTs coatings with 3D printing technology, has developed a novel airway stent and showcased its advantages in antibacterial activity and suppression of granulation tissue formation in both in vitro and in vivo experiments. These findings provide an effective innovative solution for addressing stent-related complications. In the future, further optimization of stent materials and structures,

as well as enhanced research on antimicrobial biofilm properties and more clinical validation trials, will help improve the therapeutic outcomes of airway stents and facilitate their broader clinical application.

Materials and methods

Preparation of AgNPs/CNTs coated airway stents

Synthesis of AgNPs/CNTs

Carboxylated multi-walled carbon nanotubes (MWCNTs) (200 mg) were dispersed in 90 mL of deionized water using an ultrasonic bath for 60 min. $AgNO_3$ solution (10 mL, 0.8 M) was then added dropwise to the dispersion, followed by an additional 30 min of sonication to ensure uniform dispersion. The mixture was stirred for 10 h using a magnetic stirrer at 600 rpm. Ultraviolet radiation (80 W) was applied for 5 h to initiate an in-situ reduction reaction, converting Ag^+ to Ag^0 nanoparticle. After three washing cycles, the AgNPs/CNTs composite was collected by vacuum filtration and dried under vacuum at 80 °C for 8 hours[33].

Fabrication of silicone tracheal stents coated with AgNPs/CNTs

Figure 1 illustrates our printing-spraying-transfer process[33]. First, as illustrated in Fig. 1a, a mold was fabricated using a desktop fused deposition modeling (FDM) 3D printer (PanowinF1, Panowin Technology Co., Ltd., Shanghai, China) with polylactic acid (PLA) filament as the printing material. The inner wall of the mold was then coated with a thin layer of PDMS via dip-coating, followed by thorough curing in an oven at 50 °C. This PDMS layer served the dual purpose of smoothing the mold's inner surface and acting as an inert intermediate layer for in-mold transfer, thereby enhancing the transfer efficiency of AgNPs/CNTs coating. Next, the prepared AgNPs/CNTs powder was ultrasonically dispersed in anhydrous ethanol to obtain a stable suspension, which was evenly sprayed onto the mold's inner wall using an spray gun (Avalon LPH-50, China) with a 0.4 mm nozzle, as shown in Fig. 1b. For optimal coating uniformity, the nozzle was positioned 20 cm from the mold surface, the atomizing gas pressure was maintained at approximately 0.05 MPa, and the substrate temperature was set to 70 °C. Subsequently, the AgNPs/CNTs coating on the PDMS layer was transferred onto the stent surface via in-mold transfer, as illustrated in Fig. 1c. Specifically, the upper mold, lower mold, and core mold from the previous step, each bearing the sprayed AgNPs/CNTs layer, were assembled. A two-component liquid silicone mixture (1:1 ratio) was then cast into the mold. The assembly was left at room temperature for 24 h to allow slow vulcanization, enabling gradual penetration of the silicone into the AgNPs/CNTs layer. Finally, upon demolding, a silicone tracheal stent with an outer surface coated in an antibacterial AgNPs/CNTs layer was obtained, as shown in the upper left inset of Fig. 1d. The stent was gently removed from the mold, transferring the AgNPs/CNTs coating onto its outer wall. It was then subjected to a secondary curing process in an oven at 90 °C for over 4 h, resulting in the final stent with a firmly adhered antibacterial coating. Although the fabricated mold possesses a relatively simple structure, the use of 3D printing facilitates rapid prototyping and dimensional standardization, thereby enhancing the stability and consistency of subsequent batch experiments.

Characterization and properties of AgNPs/CNTs

A range of advanced material characterization techniques—including scanning electron microscopy , transmission electron microscopy, X-ray diffraction (XRD), thermogravimetric analysis, and X-ray photoelectron spectroscopy —have been employed in previous studies to elucidate the structural and physicochemical characteristics of AgNPs/CNTs. These analyses revealed a characteristic fibrous morphology, with silver nanoparticles uniformly distributed along the surface of MWCNTs and no evident aggregation, indicating excellent dispersion and structural stability. Elemental composition assessments confirmed the presence of carbon, oxygen, and silver. The silver nanoparticles exhibited a face-centered cubic crystalline phase and primarily existed in their metallic state. Notably, the silver content measured by both TGA and energy-dispersive X-ray spectroscopy was consistent, underscoring the efficiency of the deposition process. Furthermore, oxygen-containing functional groups on the surface of MWCNTs promoted the electrostatic anchoring of silver nanoparticles, thereby improving their loading efficiency. Collectively, these findings indicate that AgNPs/CNTs feature a uniform architecture, desirable physicochemical stability, and significant antibacterial potential—attributes that make them promising candidates for the development of next-generation antimicrobial materials[33].

In vitro antibacterial evaluation of AgNPs/CNTs-coated airway stents

Bacterial activation

Staphylococcus aureus (ATCC 25,923, China Center for Type Culture Collection) and *Pseudomonas aeruginosa* (ATCC-27853, China Center for Type Culture Collection) strains, cryopreserved at − 80 °C, were gently thawed. Using a sterile inoculation loop, a small amount of each strain was transferred from the cryovials into test tubes containing 2 ml of LB medium, which were then gently agitated to fully suspend the bacteria. A 100 µl aliquot of the bacterial suspension was streaked onto blood agar plates using the four-quadrant streaking method. Plates were incubated at 37 °C in a 5% CO_2 atmosphere for 18–24 h. Colony morphology was monitored to ensure bacteria remained in the logarithmic growth phase—*Staphylococcus aureus* typically forms golden or white colonies, while *Pseudomonas aeruginosa* exhibits green or blue-green pigmentation. After incubation, revived strains were again streaked onto blood agar plates and incubated for another 18–24 h to prepare for further assays.

Disc diffusion assay

(1) Preparation of Bacterial Suspension: Sterile throat swabs were used to collect samples from subcultured *Staphylococcus aureus* and *Pseudomonas aeruginosa* colonies and suspended in 3 ml of saline. Turbidity was adjusted using a densitometer to 0.5 McFarland standard (approx. 1.5×10^8CFU/ml).

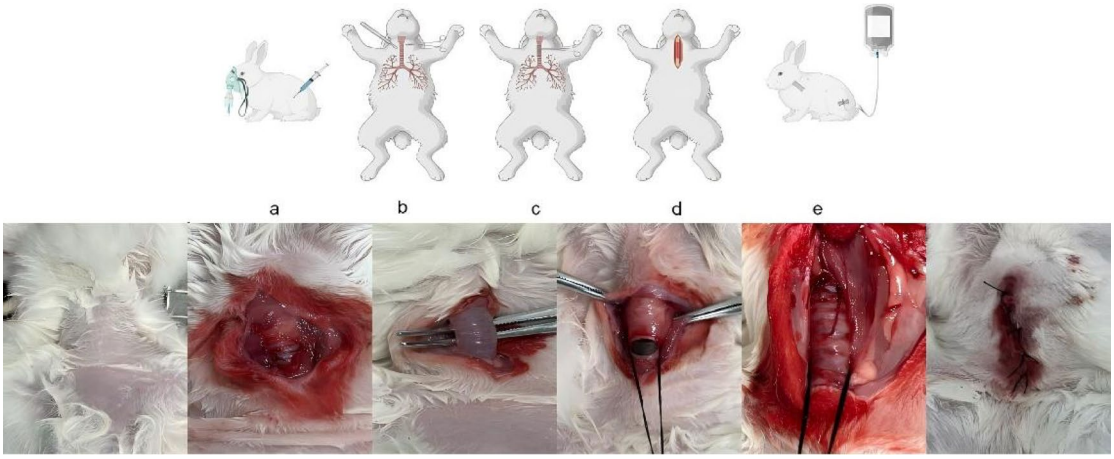

Fig. 10. Preparation of rabbit airway scaffold implantation model. (**a**) Inhalation anesthesia and intramuscular injection anesthesia were administered based on the rabbit's body weight; (**b**) A midline incision was made at the neck, and the trachea was exposed layer by layer; (**c**) A transverse incision was made on the trachea, and the airway scaffold was implanted; (**d**) Layer-by-layer suturing was performed using monofilament thread; (**e**) Postoperative recovery was conducted, and intravenous antibiotics were administered to prevent infection.

(2) Bacterial Inoculation: Sterile swabs were immersed in the adjusted suspension, gently pressed against the tube wall to remove excess fluid, and evenly spread onto Mueller–Hinton (MH) agar plates in a crosswise pattern, followed by circular streaking along the plate edges to ensure uniform distribution.
(3) Placement of Test Discs: Sterile forceps were used to place filter paper discs soaked with AgNPs/CNTs solution or saline (6.02 wt% AgNPs/CNTs and 0.9% NaCl) onto the inoculated MH agar. Each group received three replicates. Plates were incubated at 37 °C with 5% $CO_2$for 18–24 h. After incubation, zones of inhibition were measured using Image-Pro Plus software (Media Cybernetics, Silver Spring, USA).

Colony counting post co-culture

(1) Preparation of LB Bacterial Suspension: A 50 µl aliquot of 0.5 McFarland standard bacterial suspension was added to 4.95 ml LB broth to achieve 10^6CFU/ml, thoroughly mixed by pipetting.
(2) Co-culture with Stents: AgNPs/CNTs-coated and uncoated silicone airway stents were immersed in 5 ml bacterial suspension (10^5 CFU/ml) and incubated on a shaking incubator at 37 °C for 24 h.
(3) Post Co-Culture Colony Count: Bacterial suspensions were serially diluted in tenfold steps. Ten microliters of each dilution were plated on nutrient agar in triplicate and incubated at 37 °C with 5% $CO_2$for 24–48 h. Colonies were counted, and bacterial survival was expressed as CFU/ml. Inhibition rate (%) was calculated as:

$$\text{Inhibition rate} = [(\text{Control CFU} - \text{Experimental CFU})/\text{Control CFU}] \times 100\%$$

In vivo antibacterial evaluation of AgNPs/CNTs-coated airway stents

Experimental animals and grouping

All surgical procedures were approved by the Animal Care Committee of Zhejiang Chinese Medical University, adhering to the NIH Guidelines for the Care and Use of Laboratory Animals. A total of 26 female New Zealand White rabbits (2.5–3.0 kg) were procured from the university's animal center. Animals were monitored to ensure absence of systemic disease. Using a random number table, rabbits were assigned to three groups: 2 served as a blank group with tracheotomy but no stent implantation, and the remaining 24 were randomly divided into a control group (uncoated stents) and experimental group (AgNPs/CNTs-coated stents), with 12 rabbits per group.

Construction of animal airway stent model

(1) Anesthesia: Animals were fasted for 6 h preoperatively. General anesthesia was induced via intramuscular ketamine (0.5 mg/kg) and inhaled isoflurane (1–2%). Loss of reflexes and muscle tone confirmed anesthetic depth.
(2) Stent Implantation: Rabbits were positioned supine and limbs fixed. The neck and thorax were shaved and sterilized. A midline cervical incision exposed the trachea. A transverse incision (2/3 of the tracheal ring) was made 2 cm below the cricoid cartilage. Silicone stents (coated or uncoated) were inserted and fixed using fine absorbable sutures. The incision was closed in layers. (Procedure illustrated in Fig. 10)
(3) Postoperative Management: Rabbits were monitored post-surgery and returned to the animal center upon stable respiration. Cefazolin (0.1 ml/kg, intramuscularly) was administered 40 min pre-op and 24 h post-op for infection prophylaxis. Meloxicam (0.2 mg/kg) was given postoperatively for analgesia.

Plate colony counting

(1) Sample Collection: At weeks 2 and 4 post-implantation, bronchoalveolar lavage was performed using 10 ml sterile saline. One milliliter of retrieved lavage fluid was reserved for bacterial analysis.
(2) Colony Counting: The lavage fluid was serially diluted tenfold. Ten microliters of each dilution were plated on nutrient agar in triplicate and incubated at 37 °C with 5% $CO_2$for 24–48 h. Colony counts were recorded after visible growth.

Biofilm quantification

(1) Sample Fixation: At week 4, stents were retrieved, rinsed with PBS to remove planktonic bacteria, and fixed in 4% paraformaldehyde for 15–30 min at room temperature. Samples were then washed thrice with PBS.
(2) Staining and Imaging: FITC-ConA solution (50 μg/ml in PBS) was prepared. Stents were immersed and stained for 30–60 min in the dark with gentle agitation. Samples were then washed, blotted dry, and scanned using confocal microscopy. Biofilm distribution and thickness were analyzed with ZEISS ZEN (Carl Zeiss Microscopy GmbH, Jena, Germany) software.

Histopathological evaluation of tracheal tissue

Four weeks following tracheal stent implantation, the rabbits were humanely euthanized via inhalation of pure carbon dioxide. Transverse incisions were made at the proximal and distal ends of the stented trachea to facilitate stent removal. The tracheal specimens were then rinsed with 0.9% saline and subsequently fixed in 4% paraformaldehyde solution for 24 h. After paraffin embedding, the samples were sectioned and stained using hematoxylin and eosin (HE) and Masson's trichrome stain (MTS) for histopathological analysis. The thickness of granulation tissue was measured using ImageJ software. Based on previous studies[28,34,35], the degree of inflammation and collagen deposition was evaluated via H\&E and MTS staining. Key parameters for assessing tracheal pathology included granulation tissue thickness, inflammatory cell infiltration, and collagen accumulation[36,37]. Inflammatory response was graded on a five-point scale according to the distribution and density of infiltrating cells: Grade 1 (mild), Grade 2 (mild to moderate), Grade 3 (moderate), Grade 4 (moderate to severe), and Grade 5 (severe). Collagen deposition was scored subjectively using the following scale: 1 = mild, 2 = mild to moderate, 3 = moderate, 4 = moderate to severe, and 5 = severe. The extent of tracheal stenosis was thus estimated by quantifying these three indices.

Statistical analysis

Statistical analysis was performed using GraphPad Prism 8.0 (GraphPad Inc., San Diego, CA, USA). Data that followed a normal distribution were expressed as mean ± standard deviation (Mean ± S.D.), while non-normally distributed data were presented as median (25%, 75%). Data analysis was performed using an independent t-test. When the P value was < 0.05, the results were considered statistically significant.

Data availability

All data generated or analysed during this study are included in this published article and its supplementary information files.

Received: 25 February 2025; Accepted: 10 September 2025
Published online: 14 October 2025

References

1. Abia-Trujillo, D. et al. Central airway collapse, an underappreciated cause of respiratory morbidity. *Mayo Clin. Proc.* **95**, 2747–2754 (2020).
2. Schulze, A. B. et al. Central airway obstruction treatment with self-expanding covered Y-carina nitinol stents: A single center retrospective analysis. *Thorac. Cancer* **13**, 1040–1049 (2022).
3. Lin, L. Q. et al. Long-term efficacy and safety of the dumon stent for treatment of benign airway stenosis. *Ther. Adv. Respir. Dis.* **17**, 174534666231181280 (2023).
4. Aktaş, Z., Öztürk, A., Yılmaz, A., Kızılgöz, D. & Yurtseven, G. Complications of silicone Y stents placed due to malignant airway stenosis. *Tuberk. Toraks* **67**, 22–30 (2019).
5. Li, Z. et al. Synergistic effects of silver nanoparticles and cisplatin in combating inflammation and hyperplasia of airway stents. *Bioact. Mater.* **9**, 266–280 (2022).
6. Liu, H. Y., Prentice, E. L. & Webber, M. A. Mechanisms of antimicrobial resistance in biofilms. *Npj Antimicrob. Resist.* **2**, 27 (2024).
7. Mishra, V. et al. Pharmaceutical aspects of green synthesized silver nanoparticles: A boon to cancer treatment. *Anti-Cancer Agents Med. Chem.* **21**, 1490–1509 (2021).
8. Casals, E., Gusta, M. F., Bastus, N., Rello, J. & Puntes, V. Silver nanoparticles and antibiotics: A promising synergistic approach to multidrug-resistant infections. *Microorganisms* **13**, 952 (2025).
9. Lu, X. et al. Simulation and fabrication of carbon nanotube–nanoparticle interconnected structures. *Mech. Sci.* **12**, 451–459 (2021).
10. Hakkenbrak, N. A., Truijers, M. & Thomassen, I. Thoracic endovascular aneurysm repair and tracheal stenting for respiratory failure due to a thoracic aortic aneurysm: A case report. *Vasc. Endovasc. Surg.* **56**, 514–516 (2022).
11. Shan, Q. et al. Treatment of aerodigestive fistulas with a novel covered metallic Y-shaped segmented airway stent customized with the assistance of 3D printing. *Ann. Transl. Med.* **9**, 1051 (2021).
12. Smith, M. M. & Buck, L. S. Update on the diagnosis and management of pediatric laryngotracheal stenosis. *Expert Rev. Respir. Med.* **16**, 1035–1041 (2022).
13. Chang, X. et al. Silver nanoparticles induced cytotoxicity in HT22 cells through autophagy and apoptosis via PI3K/AKT/mTOR signaling pathway. *Ecotoxicol. Environ. Saf.* **208**, 111696 (2021).
14. Dunlap, D. G., Ravenel, J., Sechrist, J. & Semaan, R. Interventional therapies for central airways. *J. Thorac. Imaging* **34**, W49–W59 (2019).

15. Swolana, D. et al. The antibacterial effect of silver nanoparticles on staphylococcus epidermidis strains with different biofilm-forming ability. *Nanomaterials* **10**, 1010 (2020).
16. Dawson, L. F. et al. Extracellular DNA, cell surface proteins and c-di-GMP promote biofilm formation in clostridioides difficile. *Sci. Rep.* **11**, 3244 (2021).
17. McGinniss, J. E. et al. Molecular analysis of the endobronchial stent microbial biofilm reveals bacterial communities that associate with stent material and frequent fungal constituents. *PLoS ONE* **14**, e0217306 (2019).
18. Siddique, M. H. et al. Effect of silver nanoparticles on biofilm formation and EPS production of multidrug-resistant klebsiella pneumoniae. *Biomed. Res. Int.* **2020**, 6398165 (2020).
19. Dsouza, F. P., Dinesh, S. & Sharma, S. Understanding the intricacies of microbial biofilm formation and its endurance in chronic infections: A key to advancing biofilm-targeted therapeutic strategies. *Arch. Microbiol.* **206**, 85 (2024).
20. Montaser, A. S., Jlassi, K., Ramadan, M. A., Sleem, A. A. & Attia, M. F. Alginate, gelatin, and carboxymethyl cellulose coated nonwoven fabrics containing antimicrobial AgNPs for skin wound healing in rats. *Int. J. Biol. Macromol.* **173**, 203–210 (2021).
21. Ciriminna, R., Albo, Y. & Pagliaro, M. New antivirals and antibacterials based on silver nanoparticles. *ChemMedChem* **15**, 1619–1623 (2020).
22. Chen, C.-Y. et al. Ångstrom-scale silver particle-embedded carbomer gel promotes wound healing by inhibiting bacterial colonization and inflammation. *Sci. Adv.* **6**, eaba0942 (2020).
23. Adeyemi, O. S., Shittu, E. O., Akpor, O. B., Rotimi, D. & Batiha, G.E.-S. Silver nanoparticles restrict microbial growth by promoting oxidative stress and DNA damage. *EXCLI J.* **19**, 492–500 (2020).
24. Mendez-Pfeiffer, P. et al. Chitosan-coated silver nanoparticles inhibit adherence and biofilm formation of uropathogenic escherichia coli. *ACS Infect. Dis.* **10**, 1126–1136 (2024).
25. Lam, P.-L. et al. The role of reactive oxygen species in the biological activity of antimicrobial agents: An updated mini review. *Chem.-Biol. Interact.* **320**, 109023 (2020).
26. Tăbăran, A.-F. et al. Silver nanoparticles for the therapy of tuberculosis. *Int. J. Nanomed.* **15**, 2231–2258 (2020).
27. Xu, J. et al. Enhanced antibacterial and anti-biofilm activities of antimicrobial peptides modified silver nanoparticles. *Int. J. Nanomed.* **16**, 4831–4846 (2021).
28. Flumignan, V. K. et al. Comparison between biliary plastic stents with and without application of silver nanoparticles: an in-vitro study of the biofilm formation. *Acta Cir. Bras.* **40**, e402825 (2025).
29. Ansari, M. A. et al. Counteraction of biofilm formation and antimicrobial potential of terminalia catappa functionalized silver nanoparticles against candida albicans and multidrug-resistant gram-negative and gram-positive bacteria. *Antibiotics* **10**, 725 (2021).
30. Shan, Q. et al. Preliminary experience with a novel metallic segmented transcordal stent modified with three-dimensional printing for inoperable malignant laryngotracheal stenosis. *Front. Oncol.* **11**, 619781 (2021).
31. Yin, I. X. et al. Developing biocompatible silver nanoparticles using epigallocatechin gallate for dental use. *Arch. Oral Biol.* **102**, 106–112 (2019).
32. Yamabe, A. et al. Development of biliary stent applying the antibacterial activity of silver: A literature review. *Bio-Med. Mater. Eng.* **32**, 63–71 (2021).
33. Liu, J. et al. A printing-spray-transfer process for attaching biocompatible and antibacterial coatings to the surfaces of patient-specific silicone stents. *Biomed. Mater.* **15**, 55036 (2020).
34. Jun, E. J. et al. EW-7197, an activin-like kinase 5 inhibitor, suppresses granulation tissue after stent placement in rat esophagus. *Gastrointest. Endosc.* **86**, 219–228 (2017).
35. Park, W. et al. Metallic stent mesh coated with silver nanoparticles suppresses stent-induced tissue hyperplasia and biliary sludge in the rabbit extrahepatic bile duct. *Pharmaceutics* **12**, 563 (2020).
36. Park, J.-H. et al. Nanofunctionalized stent-mediated local heat treatment for the suppression of stent-induced tissue hyperplasia. *ACS Appl. Mater. Interfaces* **10**, 29357–29366 (2018).
37. Olmos-Zuñiga, J. R. et al. Treatment with hyaluronic acid and collagen-polyvinylpyrrolidone improves extracellular matrix assembly for scarring after tracheal resection. *Biomed Res. Int.* **2020**, 3964518 (2020).

Author contributions

Conceptualization, YJ, YXY and HXH; methodology, HXH, ZBZ and FKY; validation, HXH; formal analysis, HXH and PTY; investigation, HXH and LTF; resources, YJ and YXY; funding acquisition, YJ and YXY; data curation,HXH; writing—original draft preparation, HXH and ZBZ; writing—review and editing, YJ, YXY and HXH; visualization, HXH; project administration, HXH and FKY. All authors have read and agreed to the published version of the manuscript.

Funding

This work was financially supported by the Public Welfare Technology Application of Zhejiang Province [NO. LGF21H010006] and the National Natural Science Foundation of China [NO.52175278],

Declarations

Competing interests

The authors declare no competing interests.

Institutional review board statement

The Ethical Committee approved the animal study protocol for study no. IACUC-202311-21, passed in resolution by the Local Ethical Committee in Zhejiang, China, on 27 November 2023.

Ethical approval

This study adheres to the ARRIVE (Animal Research: Reporting In Vivo Experiments) guidelines to ensure transparency and scientific integrity. All animal experimental procedures were performed in compliance with the relevant ethical standards and were approved by the Animal Ethics Committee of Zhejiang Chinese Medical University.

Additional information

Supplementary Information The online version contains supplementary material available at https://doi.org/1

0.1038/s41598-025-19694-0.

Correspondence and requests for materials should be addressed to X.Y. or J.Y.